Journal of Applied Fluid Mechanics, Vol. 9, No. 6, pp. 2635-2645, 2016.
Available online at www.jafmonline.net, ISSN 1735-3572, EISSN 1735-3645.
DOI: 10.29252/jafm.09.06.25530

Wave Energy Dissipation by Permeable and Impermeable Submerged Breakwaters

Y. Ryu[1], D. Hur[2], S. Park[3], H. Chun[3] and K. Jung[3†]

[1] *Hydro Science & Engineering Research Institute, Korea Institute of Civil Engineering and Building Technology, Goyang 411-712, Republic of Korea*

[2] *Dept. of Ocean Civil Engineering (Institute of Marine Industry), Gyeongsang National University, Tongyeong 650-160, Republic of Korea*

[3] *Dept. of Naval Architecture and Ocean Engineering, Pusan National University, Busan 609-735, Republic of Korea*

†*Corresponding Author Email: kjung@pusan.ac.kr*

(Received August 24, 2015; accepted May 15, 2016)

ABSTRACT

The purpose of this study was to investigate the effect of the porosity of a submerged breakwater on wave fields, including snapshots of the wave, velocity profiles of the water over the structure, and the kinetic energy of the wave. Two-dimensional experiments were conducted for submerged trapezoidal breakwaters with impermeable and permeable layers in a two-dimensional wave tank. The flow fields obtained by the particle image velocimetry (PIV) technique are presented to understand the flow characteristics due to the waves' interactions with the submerged impermeable and permeable breakwaters, and these characteristics showed that the vertical velocity dominant flow occurred under the crest of the wave. In addition, the kinetic energies were compared for different porosities and wave conditions. The comparisons of the wave flow fields and kinetic energy distributions showed that the different pattern of the dissipated kinetic energy was dependent on the porosity. The dissipation of kinetic energy also was observed to increase as the wave period increased. The comparisons indicated that greater amounts of energy were dissipated for longer wave periods.

Keywords: Submerged breakwater; Velocity profile; Energy dissipation; Kinetic energy; Permeability.

NOMENCLATURE

KE	kinetic energy	H	wave height
η	wave elevation	T	wave period
u	horizontal velocity component	k	Wave number
w	vertical velocity component	A	wave amplitude
ds	the z coordinate of the structure surface	L	wave length
d	water depth		

1. INTRODUCTION

Breakwaters are constructed to protect coastal areas from waves. Among the various kinds of breakwaters, a submerged breakwater allows waves to transmit to the rear side. Although a submerged breakwater reduces the impacts of waves to a lesser extent than other types, it has the advantage of maintaining better water quality or a view of the landscape. It also provides a habitat for marine life and allows sediment to be transported onto the beaches. A submerged breakwater is usually built as a rubble stone mound type or an armour-unit one on the seabed. Since wave fields and energy transmission or dissipation can be influenced by the porosity of a submerged breakwater as well as its geometrical conditions, the porosity of breakwater materials is of importance in terms of the hydrodynamic behavior of the water flowing over the breakwater.

Many studies of submerged breakwaters have

focused on wave deformation, wave energy dissipation, and wave forces due to the interactions of the wavers. The deformation of waves by submerged breakwaters has been examined with various wave parameters since the energy dissipation and transmission can be estimated from changes in the wave profile. Wave deformation related to transmission and reflection due to a submerged breakwater or a low-crested structure has been the subject of many experimental and numerical studies. For example, d'Angremond *et al.* (1996) examined the wave transmission coefficient for various structural shapes and wave parameters. Grilli et al. determined wave transmission and reflection coefficients experimentally, including the investigation of the breaking behavior of solitary waves over breakwaters (Grilli *et al.* 1994). Kramer *et al.* (2005) studied flow velocities inside and close to a permeable breakwater for the wave obliquity in a 3D wave basin. Meer *et al.* (2000) investigated wave transmission over a low-crested dam with wave periods and spectral changes having influence on the design of the structure. Carevic *et al.* (2013) also studied the relationship between wave parameters, such as wave period and wave steepness, and wave profile measurements. Some experimental studies (Saitoh *et al.* 2001; Stansby *et al.* 2004) presented wave velocity fields over submerged breakwaters using various measurement techniques. Their approaches focused mainly on describing the flow patterns. Submerged breakwaters also have been investigated in various numerical studies (Hur *et al.* 2008; Jeng 2003; Kawasaki 1999). Although numerical studies can provide detailed flow properties, the focus has been on pressure information because the other properties that have been estimated by numerical models have not been verified experimentally.

Since a rubble mound breakwater consists of various layers of materials, the interactions with armour units or stones are important. The porous layers of a breakwater cause various hydrodynamic problems. Wave forces acting on armour stones were investigated by Rufin *et al.* (1996) from the stability perspective. The interaction between the seabed and a breakwater due to pore water pressure also has been investigated (Hur *et al.* 2008; Nago *et al.* 1993; Zen *et al.* 1990). Many numerical studies (Hur *et al.* 2008; Hur *et al.* 2010; Mizutani *et al.* 1998; Yamamoto *et al.* 1978) have reported the quantified results of the integrated wave–structure–seabed interaction problem. Wave overtopping and transformation through a low-crest breakwater also have attracted the interest of many researchers. Recently, Sierra *et al.* (2010) introduced an energetic wave propagation model that improved the simulations of wave transformation and wave overtopping of permeable coastal structures. Shao (2010) conducted incompressible smoothed particle hydrodynamics (SPH) modeling to simulate waves over porous media, which is a typical type of layer in a low-crested breakwater. Zou and Peng (2011) used the 2-D RANS-VOF model to study wave skewness and investigate wave nonlinearity over a submerged structure. Laboratory studies of the wave-structure-seabed interaction were conducted recently (Bierawski *et al.* 2003; Mizutani *et al.* 1998), but they were unable to provide detailed results of the problem due to difficulties encountered in measuring flow properties and pressures through pores.

Wave deformation and energy dissipation by a submerged breakwater have been the primary topics of related studies. Since energy dissipation is estimated indirectly by using wave elevation data, deformations in the wave elevation resulted in changes of the potential energy. However, it is difficult to estimate the variations of kinetic energy from the incoming and transmitted wave elevation data. To investigate the variation of kinetic energy over a submerged breakwater in this study, the velocity fields under the wavy free surface were obtained using the PIV technique. Flow characteristics and kinetic energy distributions on the model structure were measured and computed over one wave period for each wave condition. In addition, impermeable and permeable structures were tested to determine the hydrodynamic effect of the porosity layer by comparing the velocity fields and the kinetic energy for different porosity conditions.

2. MATERIALS AND METHODS

The experiments were conducted in a two-dimensional wave tank, which was 35.0 m long, 1.0 m wide, and 1.2 m deep (Fig. 1). Throughout the experiments, the water depths were kept constant at d = 0.50 m near the wavemaker and at d = 0.35 m in the vicinity of the measurement section. The glass-wall wave flume was equipped with a piston-type wave maker and a sloped (1/2.1) wave absorber was installed at the other end of the tank to reduce wave reflection. Most absorbers in a 2D wave flume have slopes less than 1:5 (Khalilabadi *et al.* 2012).

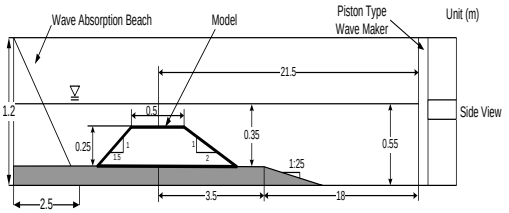

Fig. 1. Submerged breakwater model in the wave flume.

A structure modeling a submerged breakwater was installed on the bottom at 21.5 m away from the wavemaker, as shown in Fig. 1. The two-dimensional submerged breakwater model was trapezoidal-shaped and had a height of 0.35 m, a top length of 0.50 m, and a bottom length of 1.38 m. The front slope of the model structure was 1V:2H, and the rear slope was 1V:1.5H, which was scaled down from submerged breakwaters generally constructed along a coastal region. The impermeable breakwater model was made of wood

boards, and the permeable breakwater model was made with one of the armour units, tetrapod (TTP). The porosity of the permeable breakwater was determined from the armour unit, and it was 50%. Fig. 1 shows a schematic view of the breakwater model in the wave flume.

Monochromatic waves were tested in the experiments to investigate the flow characteristics over the submerged breakwater. To understand the characteristics of the flow field for various wave periods, the experiments were conducted with three wave periods (T = 1.0, 1.3, and 1.6 s). Each wave period had different wave heights (H) for different wave steepness. Table 1 provides the wave conditions at the measurement site. To avoid the wave reflection effect and the initial transient waves, the PIV measurements were acquired after initially passing three waves and before the waves returned after being reflected from the absorbent beach at the end of the wave flume.

Table 1 Wave conditions at the measurement site

	Water depth, d (m)	Wave period, T (s)	Wave length, L (m)	Wave height, H (cm)	Wave steepness kA
Case 1	0.35	1.0	1.42	3.91	0.086
Case 2	0.35	1.3	2.07	3.34	0.051
Case 3	0.35	1.6	2.39	2.84	0.028

The particle image velocimetry (PIV) technique was used to measure the velocity fields under the waves. The PIV system used in this study was set with a continuous laser and a high speed camera. The combination of the continuous laser and high speed camera made it feasible to obtain velocity maps that had better temporal resolution during a certain period compared with the PIV system that used a pulsed laser. The continuous diode laser we used (Blitz laser, Laser Animation Sollinger) had a maximum power of 8 W, a wave length of 532 nm, and a diameter of 3 mm. Our high speed CCD camera (Motion Y5, Redlake) had a resolution of 2,352×1,728 pixels, a maximum framing rate of 7,000 frames per second (fps), and a dynamic range of 8 bits. The seeding particles illuminated by the laser had a mean size of 56 μm. Velocity profiles were computed by the correlation method between successively-captured images that had a time difference, dt. Three fields of view (FOVs) were used to obtain wide velocity profiles over the submerged breakwater model, including the front slope, top, and rear slope, as shown in Fig. 2. The FOVs were composed to represent the entire flow field over the structure. The time difference, dt, between a pair of images for each FOV was set as 4 ms to get an instantaneous maximum displacement less than a third of the interrogation areas, which gave a good correlation. The FOV information is presented in Table 2. The velocity maps calculated from the image pairs were obtained every 0.02 s, which means that 50, 65, and 80 velocity maps were captured for each wave component of T = 1.0, 1.3, 1.6 s, respectively. The PIV system was synchronized with the wavemaker by using a triggering signal and a reference signal. In addition, the raw images for PIV also were used to extract a spatial wave profile at a given moment by conducting the image analysis by digitizing the water surface illuminated by a laser light sheet.

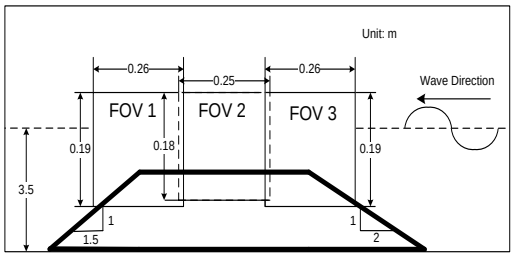

Fig. 2. Breakwater model and fields of view for PIV measurements.

Table 2 FOVs and spatial resolutions

FOV	FOV Size (mm^2)	Spatial Resolution (mm^2)	Time difference (ms)
FOV 1	190×260	3.52×3.52	4
FOV 2	180×250	3.33×3.33	
FOV 3	190×260	3.52×3.52	

3. RESULTS

3.1. Wave Snapshot

The spatial wave profiles for the wave and porosity conditions were examined. Figures 3 and 4 show the seven wave profiles of each wave condition, depending on the porosity condition. In this study, we selected the wave profiles for which the wave crest propagated over the tested region. Fig. 3 shows that the wave profiles of the impermeable condition, and they indicate that the wave elevations did not increase significantly over the seaward slope irrespective of the wave conditions. Wave development was not observed until after the top of the structure. As the wave was propagating to the leeward side over the top, the wave elevation did not increase significantly. We observed the same pattern for the wave profiles at all wave conditions. For the impermeable condition, most of the wave profiles of all wave conditions appeared to be skewed. Since the structure reduced the water depth which caused wave shoaling, the wave field could be considered to be within the wave process to wave breaking. From the shapes of the wave profiles, wave breaking was not observed. However, since the wave elevations increased as they developed over the impermeable structure, it appeared that the waves were likely to be in the process of approaching wave breaking. Fig. 4 shows the wave profiles over the permeable structure for the same wave conditions. The shape of the wave profile and wave elevation shows a

very different pattern from the impermeable condition. There was no clear skewness of the wave crest, and there was no significant increase in the wave elevation. The energy dissipation by the porous material of the structure could lead to the wave profiles.

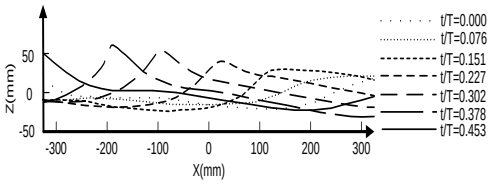

a) T = 1.0 s

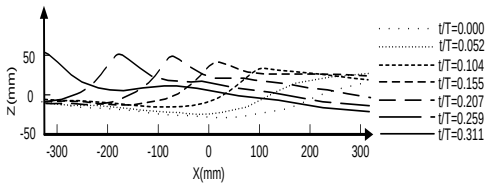

b) T = 1.3 s

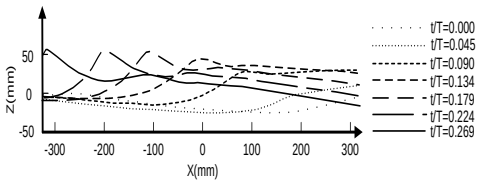

c) T = 1.6 s

Fig. 3. Spatial wave profile over the impermeable structure.

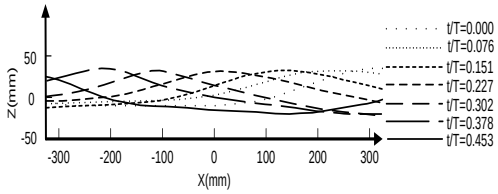

a) T = 1.0 s

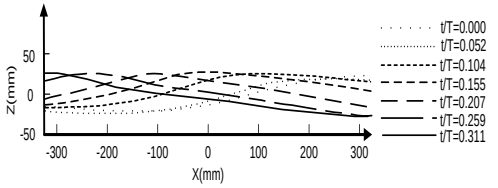

b) T = 1.3 s

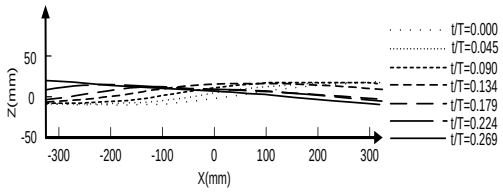

c) T = 1.6 s

Fig. 4. Spatial wave profile over the permeable structure.

3.2. Flow Field

The sequential velocity fields of the propagating wave over the permeable submerged breakwater are shown in Figs. 5 and 6. In the figures, five velocity fields, evenly chosen for all of the cases, are presented for the analysis of the wave flow field. The velocity profiles in the left and right columns represent the cases of the impermeable and permeable structures, respectively. The velocity maps present all of the velocity profiles obtained from the three fields of view (FOVs) shown in Fig. 2. Note that the origin, (x, z) = (0, 0) is at the intersection of the middle of the structure and the still water level. For each wave condition, the velocity fields over the impermeable and permeable breakwaters at the corresponding phases were compared.

Figure 5 presents the velocity fields of the case with T = 1.0 s and H = 3.94 cm, Case 1. The velocity fields of the impermeable condition had a larger magnitude than those of the permeable condition. The wave profile propagating across the breakwater was asymmetric, and the skewness of the wave profile of the impermeable condition was more notable than that of the permeable condition, which is also shown in Fig. 3. The propagation behavior of the wave crest with strong momentum appeared similar to the breaking wave, although the velocity of the front face was not horizontally dominant. Once a wave becomes skewed from the symmetrical profile of the linear theory, the wave starts to form a front face as if approaching wave breaking. In the wave process, when the wave crest reaches a certain level after increasing due to wave shoaling or wave focusing, its wave profile begins to form the front face. As the process continues, the front face of the wave over the still water level becomes steeper. When the front face becomes almost vertical, the zero up crossing point is located near the front face, which was similar to the flow fields shown from the impermeable condition in this study. In other words, the flow fields of the impermeable condition were of the phase before the wave breaking. From the velocity fields over the impermeable breakwater, it was observed that the vertical velocity components were dominant along the water column under the front face of the wave's crest. Based on the linear wave theory, the vertical distribution of the vertical velocity components is expected to occur at the zero up crossing point. The vertical velocity distribution along the water column taking place around the steep front face of the wave also explains that the impermeable structure caused the flow fields close to wave breaking. In addition, the velocity vectors under the wave trough right before the wave front face, i.e., the vectors in front of the vertical velocity column, were found to be mainly horizontal and were observed to change suddenly to the vertical velocity column. The velocity pattern showing the sudden change in the direction also indicated that the front face of the wave was almost vertical. Since the profile of the front of the wave did not have a gradually-varying shape, the velocity direction did not change smoothly either.

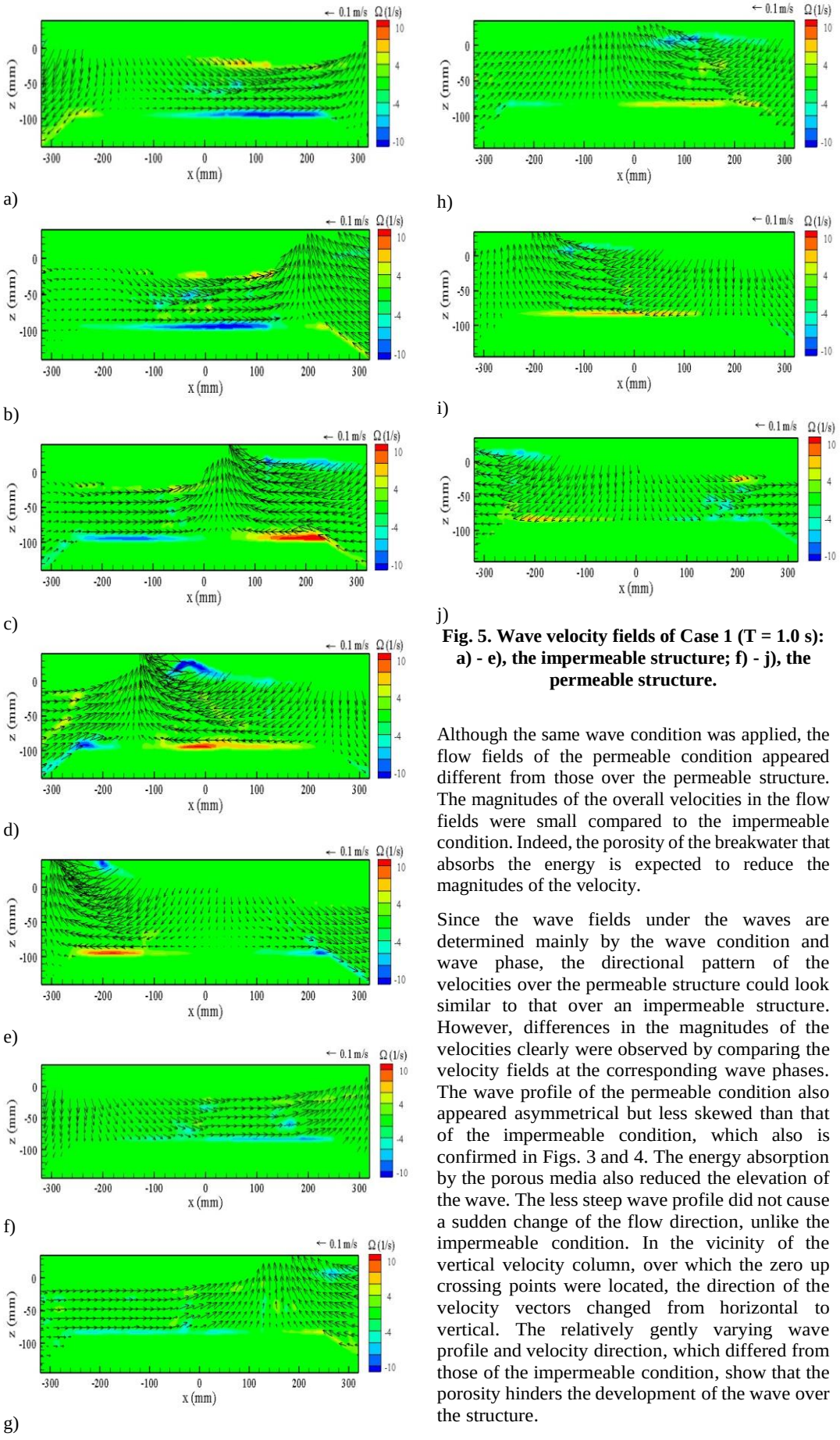

Fig. 5. Wave velocity fields of Case 1 (T = 1.0 s): a) - e), the impermeable structure; f) - j), the permeable structure.

Although the same wave condition was applied, the flow fields of the permeable condition appeared different from those over the permeable structure. The magnitudes of the overall velocities in the flow fields were small compared to the impermeable condition. Indeed, the porosity of the breakwater that absorbs the energy is expected to reduce the magnitudes of the velocity.

Since the wave fields under the waves are determined mainly by the wave condition and wave phase, the directional pattern of the velocities over the permeable structure could look similar to that over an impermeable structure. However, differences in the magnitudes of the velocities clearly were observed by comparing the velocity fields at the corresponding wave phases. The wave profile of the permeable condition also appeared asymmetrical but less skewed than that of the impermeable condition, which also is confirmed in Figs. 3 and 4. The energy absorption by the porous media also reduced the elevation of the wave. The less steep wave profile did not cause a sudden change of the flow direction, unlike the impermeable condition. In the vicinity of the vertical velocity column, over which the zero up crossing points were located, the direction of the velocity vectors changed from horizontal to vertical. The relatively gently varying wave profile and velocity direction, which differed from those of the impermeable condition, show that the porosity hinders the development of the wave over the structure.

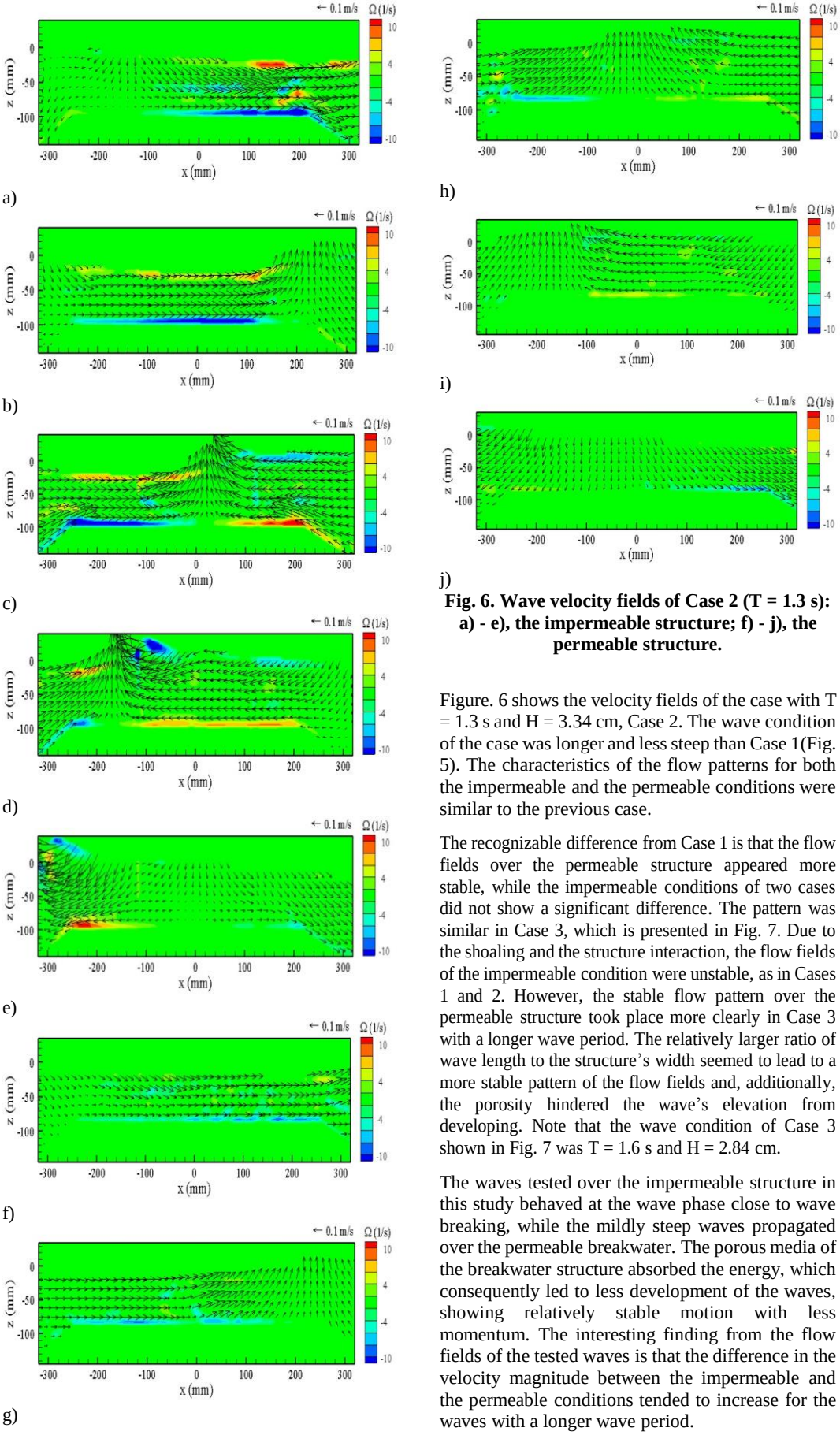

Fig. 6. Wave velocity fields of Case 2 (T = 1.3 s): a) - e), the impermeable structure; f) - j), the permeable structure.

Figure. 6 shows the velocity fields of the case with T = 1.3 s and H = 3.34 cm, Case 2. The wave condition of the case was longer and less steep than Case 1(Fig. 5). The characteristics of the flow patterns for both the impermeable and the permeable conditions were similar to the previous case.

The recognizable difference from Case 1 is that the flow fields over the permeable structure appeared more stable, while the impermeable conditions of two cases did not show a significant difference. The pattern was similar in Case 3, which is presented in Fig. 7. Due to the shoaling and the structure interaction, the flow fields of the impermeable condition were unstable, as in Cases 1 and 2. However, the stable flow pattern over the permeable structure took place more clearly in Case 3 with a longer wave period. The relatively larger ratio of wave length to the structure's width seemed to lead to a more stable pattern of the flow fields and, additionally, the porosity hindered the wave's elevation from developing. Note that the wave condition of Case 3 shown in Fig. 7 was T = 1.6 s and H = 2.84 cm.

The waves tested over the impermeable structure in this study behaved at the wave phase close to wave breaking, while the mildly steep waves propagated over the permeable breakwater. The porous media of the breakwater structure absorbed the energy, which consequently led to less development of the waves, showing relatively stable motion with less momentum. The interesting finding from the flow fields of the tested waves is that the difference in the velocity magnitude between the impermeable and the permeable conditions tended to increase for the waves with a longer wave period.

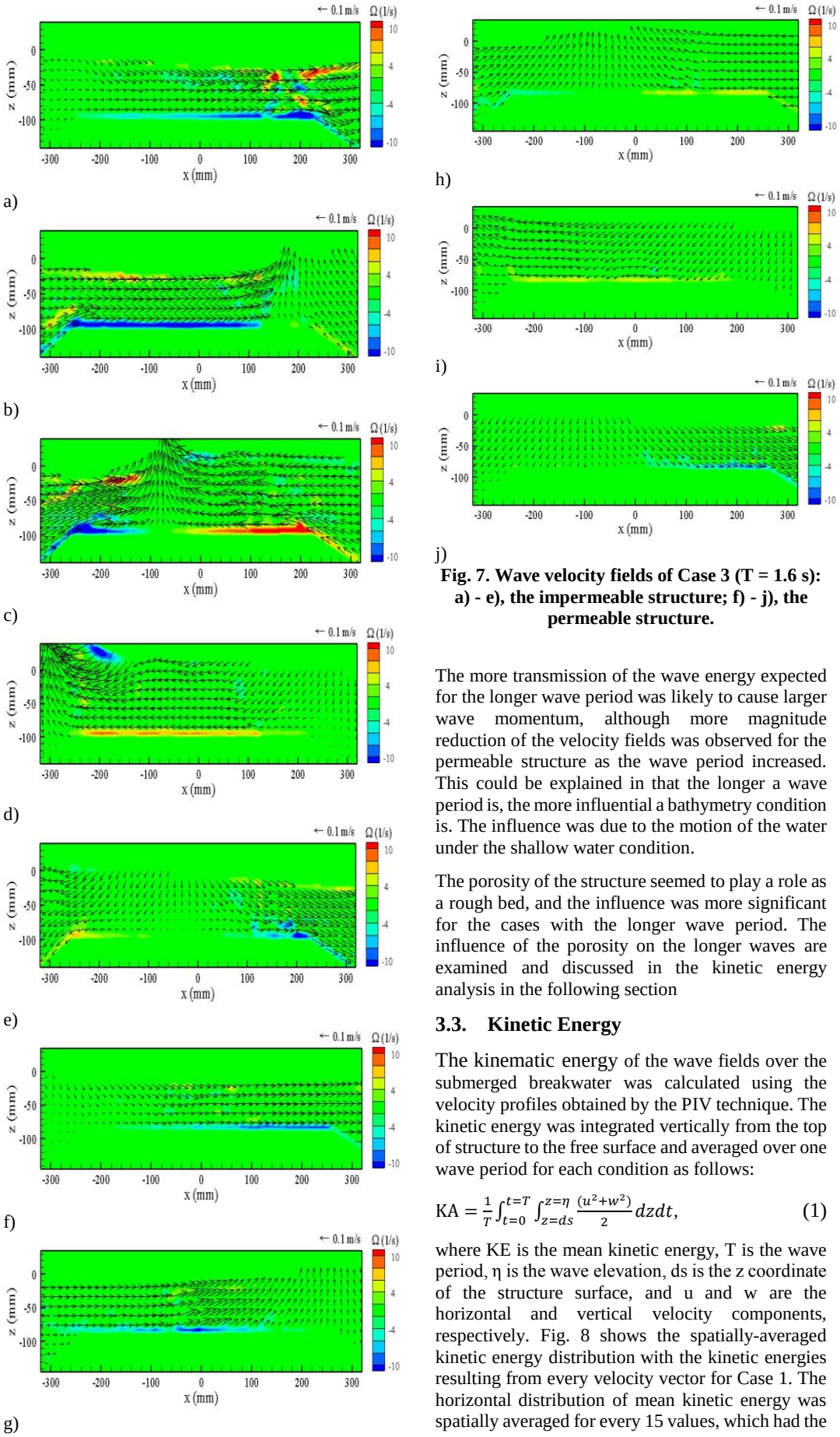

Fig. 7. Wave velocity fields of Case 3 (T = 1.6 s): a) - e), the impermeable structure; f) - j), the permeable structure.

The more transmission of the wave energy expected for the longer wave period was likely to cause larger wave momentum, although more magnitude reduction of the velocity fields was observed for the permeable structure as the wave period increased. This could be explained in that the longer a wave period is, the more influential a bathymetry condition is. The influence was due to the motion of the water under the shallow water condition.

The porosity of the structure seemed to play a role as a rough bed, and the influence was more significant for the cases with the longer wave period. The influence of the porosity on the longer waves are examined and discussed in the kinetic energy analysis in the following section

3.3. Kinetic Energy

The kinematic energy of the wave fields over the submerged breakwater was calculated using the velocity profiles obtained by the PIV technique. The kinetic energy was integrated vertically from the top of structure to the free surface and averaged over one wave period for each condition as follows:

$$\mathrm{KA} = \frac{1}{T}\int_{t=0}^{t=T}\int_{z=ds}^{z=\eta}\frac{(u^2+w^2)}{2}dzdt, \qquad (1)$$

where KE is the mean kinetic energy, T is the wave period, η is the wave elevation, ds is the z coordinate of the structure surface, and u and w are the horizontal and vertical velocity components, respectively. Fig. 8 shows the spatially-averaged kinetic energy distribution with the kinetic energies resulting from every velocity vector for Case 1. The horizontal distribution of mean kinetic energy was spatially averaged for every 15 values, which had the

spatial interval of 0.052 m. Figs. 9 - 11 present the mean kinetic energy distribution of monochromatic waves having three different wave periods for the impermeable and permeable submerged breakwaters. The figures show the differences in the magnitudes of the mean kinetic energy and distributions depending on the existence of porosity. For the three different wave periods, the mean kinetic energy over the impermeable structure was larger than that over the permeable structure, and its distribution patterns were different for the porosity conditions.

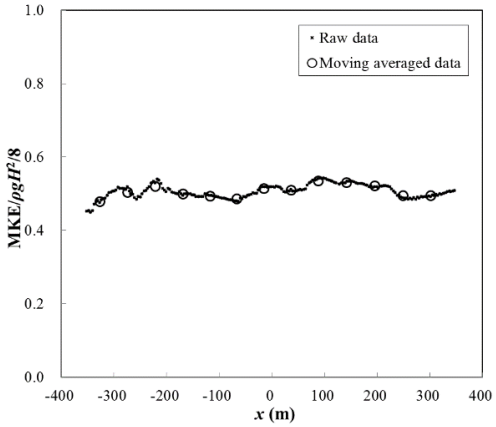

Fig. 8. Raw data and moving averaged data of kinetic energy.

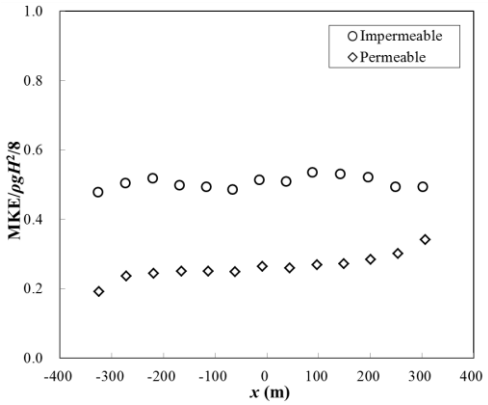

Fig. 9. Mean kinetic energy distribution of Case 1 (T = 1.0 s).

Figure. 9 shows the mean kinetic energy distributions of Case 1. In the distribution of the impermeable condition, there were two humps over the structure. The maximum mean kinetic energy was found near both corners of the top of the structure. The mean kinetic energy increased after the front corner (i.e., the seaward side) of the structure and then decreased moving downstream to the top. The increase of mean kinetic energy could be explained from wave transformation over a shallow water region. Theoretically, as waves approach a shallow water region, the wave speed decreases. If the energy flux is constant over the shallow water region, the potential energy increases. If the increase of wave height is not enough for increased potential energy, the kinetic energy is expected to increase. In this study, the wave height increase over the seaward slope of Case 1 was not large enough to contain the energy density increase and, consequently, the kinetic energy seemed to gradually increase. As the wave moved further downstream, the mean kinetic energy increased around the rear corner of the structure and decayed back over the leeward slope. However, the mean kinetic energy of the permeable condition tended to decay gradually with wave propagation from the seaward side to the leeward side of the structure for the reason of the porosity, although it had an approximately constant distribution over the top of the breakwater. The distinctive distribution patterns for both the impermeable and permeable conditions were observed from the other cases with the different wave periods and wave heights, as shown in Figs. 10 and 11. The patterns that depended on the porosity appeared similar, although the increasing or decreasing rates of mean kinetic energy were varied, depending on the wave conditions.

Although the main reason for the energy reduction or the dissimilar energy distributions could be found from the porosity conditions, other possible factors are discussed. For the impermeable condition, one of the other factors causing the distribution pattern of the mean kinetic energy could be wave reflection. Since the impermeable structure was able to partially absorb the wave's energy only with the slope, wave reflection occurred over the seaward slope. The wave reflection likely magnified the energy increase over the seaward slope. The increase of wave energy is expected to cause the increase of wave height. If the wave reflection as well as the shoaling over the impermeable surface did not increase the wave height to correspond to the energy density increase, it is assumed that the residue of increased energy density transformed to the kinetic energy as mentioned above. During wave process to wave breaking, once a wave becomes skewed, its height does not increase significantly. In this study, the wave profile and the velocity field of the case appeared to approach wave breaking. The impermeable condition and wave reflection seemed to increase the kinetic energy rather than the potential energy.

Unlike the impermeable condition, the mean kinetic energy distribution of the permeable condition showed a different pattern. Fig. 9 shows that the mean kinetic energy of the permeable condition decreased over the seaward slope of the structure. The kinetic energy increase is the predictable occurrence that the energy absorption by the permeable slope reduced the wave development and the wave reflection. In addition, the porous surface caused the roughness to the flows. The influence of porosity on kinetic energy also can be determined easily from the large difference in the magnitude of the mean kinetic energy between the impermeable and permeable conditions shown in Fig. 9. From the figures of the velocity fields, note that the water particle velocities under the less skewed wave crest of the permeable condition had smaller magnitudes than those under the more skewed wave crest of the impermeable condition at the corresponding wave phases.

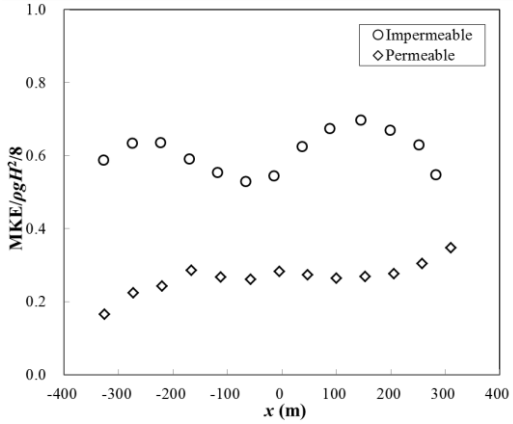

Fig. 10. Mean kinetic energy distribution of Case 2 (T = 1.3 s).

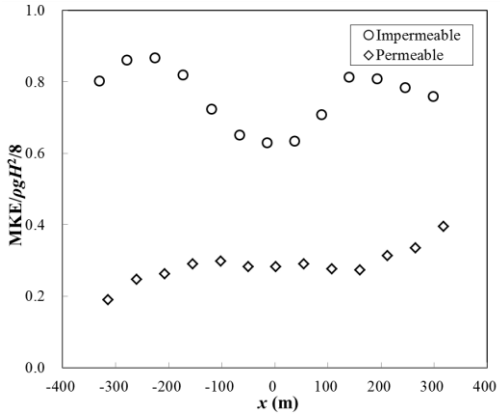

Fig. 11. Mean kinetic energy distribution of Case 3 (T = 1.6 s).

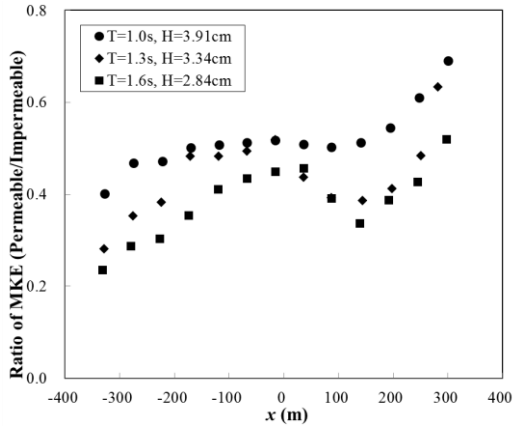

Fig. 12. Mean kinetic energy ratio between the impermeable and permeable conditions.

Another interesting observation near the front corner is that the mean kinetic energy reached a peak value at the location about 5 cm from the front corner for all the impermeable cases. Although the water depth of the water changed at the front corner, the mean kinetic energy distribution changed its increasing pattern over the top after keep increasing. A possible reason that influenced the delayed pattern could be the rapidly varying shape of the structure. Since the kinetic energy of the wave fields determined by the water particle movement would not respond immediately to the bathymetry change, the flow field development may be extended after the front corner of the structure, especially with no porosity. Although the permeable condition also showed the delaying pattern of the mean kinetic energy, the mean kinetic energy varied gradually, and the change in the distribution was not as clear as it was for the impermeable condition.

Over the top after the front slope, the mean kinetic energy of the impermeable condition showed a depression-shaped distribution. The mean kinetic energy decreased after the first peak point and then increased approaching the rear corner. The varying distribution of the mean kinetic energy seemed due to the energy conversion in which the kinetic energy was transformed into potential energy. Fig. 3 shows that, as the wave propagated over the top, the increasing wave height was observed, while the water depth was constant. Among possible factors that affected the flow field, no porosity might lead to a vigorous energy conversion. Unlike the impermeable conditions, the mean kinetic energy of the waves under the permeable condition was distributed almost constantly over the top of the structure. The distribution pattern could be caused by the less development of the waves over the porous media, since energy absorption by porous media hinders the development of waves.

Near the leeward corner of the structure with the impermeable surface, the mean kinetic energy from the depression over the top was restored and showed an increasing distribution followed by a decrease over the leeward slope. The peak of mean kinetic energy near the leeward corner appeared very similar to that near the seaward corner. Two peaks in the mean kinetic energy distribution of the impermeable conditions over the top of the structure made a shape of two humps. Since wave motion is oscillatory, the causes for the energy peak at the seaward corner could also explain the peak at the corner. Unlike the front peak, however, the rear peak also was located almost at the rear corner. There was indeed a difference in the flow pattern due to the propagation direction between the two sides. An additional difference in the conditions between the corners was the slope, i.e., the leeward slope was 1:1.5, and the seaward slope was 1:2. The possible cause for the delay of the front peak kinetic energy, for which the slope and angular corner were discussed above, would also explain the different patterns in the locations. For the steeper slope, the horizontal movement was not likely dominant compared to the less steep slope. The pattern for the impermeable condition was observed in all of the impermeable cases, as shown in Figs. 9 - 11. As the wave period increased, the difference between the maximum and minimum magnitudes of the mean kinetic energy distribution over the breakwater became larger. However, the mean kinetic energy over the permeable structure decreased after showing an approximately constant magnitude over the top. Before the decreasing pattern over the rear slope, no increase was observed in the mean kinetic energy near the rear corner, unlike the impermeable

condition. The rear decrease of mean kinetic energy started from the top of the structure.

The relative ratios of the mean kinetic energy between the impermeable and the permeable conditions for each wave condition are presented in Fig. 12, which shows that the mean kinetic energy was reduced more as the wave period increased. Since the flow velocities near the bottom relative to those around a free surface are large in a shallow water condition, the wave condition of the intermediate water depth close to the shallow water more likely would be affected by the bathymetry. The porosity of the structure, which also increases the roughness of the bottom, indeed reduced the kinetic energy to as greater extent for the longer wave conditions, which can be explained by the reduction ratios of the kinetic energy in Fig. 12. The decrease of the mean kinetic energy ratio near the front corner is due to the first peak of the mean kinetic energy distributions of the impermeable condition, as presented in Figs. 9 - 11. In addition, even though there were fluctuations in the distributions, for all of the cases, more mean kinetic energy was dissipated over the rear slope than the other regions.

4. CONCLUSIONS

In this study, we conducted experiments using the PIV technique to investigate the influence of the porosity of a trapezoidal submerged breakwater on the velocity fields and kinetic energy. Monochromatic waves with different periods and heights were generated for both the impermeable and permeable structures. The velocity fields and mean kinetic energy were compared for the different porous conditions. Under the same wave and geometry conditions, the velocity fields of the impermeable condition were very similar to wave breaking flow fields. The free surface appeared to be asymmetric, and the front surface was very steep. The velocity fields over the impermeable breakwater structure also showed spatial velocity distributions focusing the wave front face. Unlike the impermeable condition, the flow fields over the permeable structure appeared to be relatively stable, which can was apparent from the less asymmetric waver profiles and smaller velocities. As the wave periods increased, the wave fields showing the wave-breaking-like pattern were still observed from the impermeable conditions, although the wave height decreased. However, the stable appearance of the wave fields under the permeable conditions was more obvious as the wave period increased. From these observations, we can conclude that longer waves are more affected by porous media.

The mean kinetic energy also was compared for the impermeable and permeable conditions. As expected, the kinetic energy was reduced under the permeable conditions for all wave conditions. For the impermeable condition, over the front slope, the mean kinetic energy increased approaching the top of the structure. The increase might be due to no additional increases in the height of the wave. As the depth gets shallower, no wave height increase indicates that the potential energy has decreased, which may cause an increase in the kinetic energy. Unlike the impermeable case, the mean kinetic energy decreased over the front slope, which might be due to the influence of the porosity of the permeable structure. The energy dissipation can be explained from the distribution. While the mean kinetic energy of the impermeable condition was distributed similarly, its magnitude increased as the wave period increased. However, the mean kinetic energy of the permeable condition decreased, showing a similar magnitude and distribution pattern for all wave conditions. The ratio of the mean kinetic energy for the impermeable to that of the permeable conditions showed the quantitative influence on energy dissipation. Since the mean kinetic energy distribution over the breakwater structure was similar for each porosity condition, the ratio distribution pattern also was similar. As the wave period increased, the magnitude of the mean kinetic energy was reduced. The comparisons indicated that more energy dissipation occurred for longer wave periods. In this study, since the longer wave period was set with the smaller wave height, the wave energy dissipation due to the permeable structure depending on the wave period was more clearly explained.

Although this study presents an experimental approach for understanding wave flow fields and kinetic energy depending on the porosity conditions, the geometrical condition was fixed and the permeable and impermeable conditions were tested. Future studies with more experimental conditions, including wave parameters, geometry, and porosity, would be beneficial in supplementing our findings.

ACKNOWLEDGEMENTS

This work was supported by the National Research Foundation of Korea (NRF) grant funded by the Korea government (MSIP) through GCRC-SOP (No. 2011-0030013) and NRF-2009-0068310.

REFERENCES

Bierawski, L. G. and S. Maeno (2003). An experimental study on the interaction between the reef breakwater, the sandy bed and the wave field. In *30th IAHR Congr. Proc. Theme A. 377-384*

Carevic, D., G. Loncar and M. Prsic (2013). Wave parameters after smooth submerged breakwater. *Coast Eng. 79, 32–41*

d'Angremond, K., J. W. van der Meer and R. J. de Jong (1996). Wave transmission at low crested structures. In *Proc. 25th Int. Conf. Coast Eng. 3305–3318*

Grilli, S. T., M. A. Losada and F. Martin (1994). Characteristics of solitary wave breaking induced by breakwaters. *J. Waterw Port Coast Ocean Eng. 120(1), 74-92*

Hur, D. S., C. H. Kim and J. S. Yoon (2010). Numerical study on the interaction among a

nonlinear wave, composite breakwater and sandy seabed. *Coast Eng. 57(10), 917-930*

Hur, D. S., C. H. Kim, D. S. Kim and J. S. Yoon (2008). Simulation of the nonlinear dynamic interactions between waves, a submerged breakwater and the seabed. *Ocean Eng. 35(5-6), 511-522*

Jeng, D. S. (2003). Wave-induced seafloor dynamics. *Appl. Mech. Rev. 56(4), 407–429*

Kawasaki, K. (1999). Numerical simulation of breaking and post-breaking wave deformation process around a submerged breakwater. *Coast Eng. 47, 201–223*

Khalilabadi, M. R. and A. A. Bidokhti (2012). Design and Construction of an Optimum Wave Flume. *J. Applied Fluid Mech. 5(3), 99-103*

Khalilabadi, M. R. and A. A. Bidokhti (2012). Design and Construction of an Optimum Wave Flume. *J. Applied Fluid Mech. 5(3):99-103*

Kramer, M., B. Zanuttigh, J. W. Van der Meer, C. Vidal and F. X. Gironella (2005). Laboratory Experiments on Low-Crested Breakwaters. *Coast Eng. 52, 867-885*

Mizutani, N., A. M. Mostafa and K. Iwata (1998). Nonlinear regular wave, submerged breakwater and seabed dynamic interaction. *Coast Eng. 33, 177–202*

Nago, H., S. Maeno, T. Matsumoto and Y. Hachiman (1993). Liquefaction and densification of loosely deposited sand bed under water pressure variation. In *Proc. 3rd Int. Offshore Polar Eng. Conf. 578–584*

Rufin, T. M., N. Mizutani and K. Iwata (1996). Estimation method of stable weight of spherical armor unit of a submerged wide-crown breakwater. *Coast Eng. 28, 183–228*

Saitoh, T. and I. H. shida (2001). Kinematics and transformation of new type wave front breaker over submerged breakwater. In *Ocean Wave Meas. Anal. 1032-1041*

Shao, S. D. (2010). Incompressible SPH flow model for wave interactions with porous media. *Coast Eng. 57(3), 304–316*

Sierra, J. P., D. González-Marco, M. Mestres, X. Gironella, T. C. A. Oliveira, I. Cáceres and C. Mösso (2010). Numerical model for wave overtopping and transmission through permeable coastal structures. *Environ. Model and Soft 25, 1897-1904*

Stansby, P. K. and T. Feng (2004). Surf zone wave overtopping a trapezoidal structure: 1-D modeling and PIV comparison. *Coast Eng. 51, 483-500*

Van der Meer, J. W., H. J. Regeling and J. P. de Waal (2000). Wave transmission: spectral changes and its effects on run up and overtopping. In *Proc. 27th Int. Conf. Coast Eng. 2156–2168*

Yamamoto, T., H. L. Konong, H. Sellmejjer and H. L. Hijum (1978). On the response of a pore-elastic bed to water waves. *J. Fluid Mech. 87, 193–206*

Zen, K. and H. Yamazaki (1990). Mechanisms of wave-induced liquefaction and densifications in seabed. *Soils Found 30(1), 90–104*

Zou, Q. and Z. Peng (2011). Evolution of wave shape over a low-crested structure. *Coast Eng. 58, 478–488*